Structure of the *Yersinia enterocolitica* Type III Secretion Translocator Chaperone SycD

Carina R. Büttner[1], Isabel Sorg[2], Guy R. Cornelis[2], Dirk W. Heinz[1], Hartmut H. Niemann[1]*†

[1] Division of Structural Biology, Helmholtz Centre for Infection Research, Inhoffenstr. 7, D-38124 Braunschweig, Germany

[2] Division of Molecular Microbiology, Biozentrum, University of Basel, Klingenbergstraße 50/70, CH-4056 Basel, Switzerland

*Corresponding author:

† Present address: Department of Chemistry, Bielefeld University, Universitätsstraße 25, D-33615 Bielefeld, Germany

Email: Hartmut.Niemann@uni-bielefeld.de

Phon: (+49) 0521-106-6154

Fax: (+49) 0521-106–2981

Short running title : T3S translocator chaperone SycD structure

Abstract

Many Gram-negative bacteria use a type III secretion (T3S) system to directly inject effector molecules into eucaryotic cells in order to establish a symbiotic or pathogenic relationship with their host. The translocation of many T3S proteins requires specialized chaperones from the bacterial cytosol. SycD belongs to a class of T3S chaperones that assists the secretion of pore-forming translocators, and specifically chaperones the translocators YopB and YopD from enteropathogenic *Yersinia enterocolitica*. In addition, SycD is involved in the regulation of virulence factor biosynthesis and secretion. In this study, we present two crystal structures of *Y. enterocolitica* SycD at 1.95 Å and 2.6 Å resolution, the first experimental structures of a T3S class II chaperone specific for translocators. The fold of SycD is entirely α-helical and reveals three tetratricopeptide repeat (TPR)-like motifs that had been predicted from amino acid sequence. In both structures, SycD forms dimers utilizing residues from the first TPR motif. Using site-directed mutagenesis and size exclusion chromatography, we verified that SycD forms head-to-head homodimers in solution. Although in both structures, dimerization largely depends on the same residues, the two assemblies represent alternative dimers that exhibit different monomer orientations and overall shape. In these two distinct head-to-head dimers both the concave and the convex surface of each monomer are accessible for interactions with the SycD binding partners YopB and YopD. A SycD variant carrying two point mutations in the dimerization interface is properly folded but defective in dimerization. Expression of this stable SycD monomer in *Yersinia* does not rescue the phenotype of a *syc*D null mutant, suggesting a physiological relevance of the dimerization interface.

Key words:

alternative dimer assembly; chaperone; SycD; tetratricopeptide repeat; type III secretion

Abbreviations used:

T3S	Type III secretion
Yop	*Yersinia* outer protein
Syc	specific Yop chaperone
TPR	Tetratricopeptide repeat

Introduction

Several Gram-negative pathogenic and symbiotic bacteria employ T3S systems to directly inject effector molecules into host cells. Here, they modulate host cell processes that range from signal transduction to programmed cell death and cytoskeletal dynamics ensuring bacterial survival and spreading (see Mota & Cornelis [1] and Navarro *et al.* [2] for recent reviews). The secretion apparatus resembles a molecular syringe, therefore called needle-complex, and spans the bacterial inner membrane, the peptidoglycan layer and the outer membrane and ends in a needle-shaped structure (for a review see Galán & Watz [3]). Effector molecules are believed to reach the host cell by traveling through this channel. Successful translocation requires a special family of proteins, the translocators, which are also transported by the needle-complex and form a pore in the eucaryotic cell membrane allowing the effectors to enter the host cell (reviewed by Büttner & Bonas [4]).

Productive secretion of many proteins by the T3S system depends on a number of specialized chaperones. Some of the secreted proteins form specific complexes with their cognate chaperones in the bacterial cytosol but are released from the chaperone directly before secretion. According to the function of their substrates, T3S chaperones are divided into three groups [5]. Members of class I bind to effector proteins, whereas class II is dedicated to translocator proteins. A third class assists distal components of the needle complex which are themselves exported by the nascent machine. The functions of T3S chaperones are still under debate, possibly because there are different functions according to the classes and some chaperones may fulfil more than one function. Moreover, different proposed roles are not necessarily mutually exclusive (for reviews see Parsot *et al.* [5], Feldman & Cornelis [6] and Wilharm *et al.* [7]). It has been proposed that they ensure effector stabilization and prevent unproductive interactions, as well as aggregation of membrane-localization domains within the effector [8]. Further, the chaperones are suggested to maintain their binding partners in a secretion-competent, partially unfolded state [9] and to act as pilots towards the needle-

complex [10]. The effector-chaperone complex may also present a three-dimensional secretion signal and uphold a secretion hierarchy among the secretion substrates [11]. Noteworthy, several class II chaperones are also involved in the regulation of T3S-associated gene expression [12; 13; 14].

Class I and II chaperones share a small size, but unlike the effector chaperones, the representatives of class II do not exclusively possess an acidic pI. Numerous class I chaperones are structurally characterized (for a structural review on T3S see Johnson *et al*. [15]) and reveal a common mixed α/β fold despite low sequence identity. Few structures of class III members have so far been solved such as the heterodimeric PscG/PscE, binding the *Pseudomonas* needle component [16], and *E. coli* needle extension chaperone CesA [17]. However, their structural heterogeneity may justify the division into additional classes. No structure is available for class II chaperones, though tetratricopeptide repeat-like motifs have been recently identified in their sequences [18].

The three pathogenic *Yersinia* species (*Y. pestis* is the causative agent of the plague, *Y. pseudotuberculosis* and *Y. enterocolitica* are gastrointestinal pathogens) depend on their Ysc-Yop T3S system during infection. The translocated virulence factors termed *Yersinia* outer proteins (Yops) possess specific Yop chaperones (Sycs). SycD (LcrH in *Y. pestis* and *Y. pseudotuberculosis*) is the corresponding yersinial representative of class II chaperones. SycD specifically chaperones the translocator proteins YopB and YopD [19; 20]. Furthermore, SycD is involved in the modulation of the T3S system both via Yop secretion control as well as negative regulation of *yop* gene expression [21; 22; 23].

Here, we present the crystal structure of the multi-functional chaperone SycD from *Y. enterocolitica*. We furthermore identified the homodimerization interface in SycD via site-directed mutagenesis. These results provide the structural basis to rationalize previously obtained information from mutagenesis studies of SycD and its homologues.

Results

Purification, crystallization and biophysical analysis of SycD

Recombinantly produced *Y. enterocolitica* full-length SycD (19.4 kDa, 168 residues) failed to crystallize in spite of extensive screening, most likely due to its tendency to form higher oligomers (data not shown), a phenomenon also observed by other groups [24; 25]. During prolonged storage at 4 °C, SycD gradually degraded into a shorter, N-terminally truncated but stable fragment (amino acids 21-168) as determined by MALDI-TOF analysis (data not shown). The same stable fragment ($SycD_{21-168}$) was obtained by limited proteolysis with trypsin (Figure 1). Further supported by multiple sequence alignments of SycD with homologous T3S class II chaperones, secondary structure predictions and an existing structural model for the TPR domain of LcrH/SycD [18] (PDB accession code 1OOL**)**, we thus generated a shorter expression construct encompassing SycD residues 21-163. In addition to the first 20 amino acids, this construct lacks five C-terminal residues eliminating Cys164 that may cause disulfide-mediated oligomerization during crystallization.

$SycD_{21-163}$ yielded large tetragonal crystals (space group $P4_122$ or $P4_322$) diffracting to 3.8 Å at best. These crystals have a huge unit cell and Matthews coefficient probability analysis [26] suggested that the asymmetric unit most likely harbors 34 molecules. Since structure determination has failed for this crystal form, we applied reductive methylation of lysines in order to improve crystal quality or obtain a second crystal form. This method has already been applied successfully to several other T3S components [27; 28]. Lysine dimethylation resulted in a different crystal form (space group C2) of $SycD_{21-163}$ that diffracted to a resolution of 1.95 Å (Table 1). Complete modification of all 22 methylation sites in $SycD_{21-163}^{meth}$ was checked by MALDI-TOF (Figure 2a). In the new crystal form, four methylated lysines are actually

involved in crystal contacts (Figure 2b). The structure of $SycD_{21\text{-}163}^{meth}$ was finally solved by molecular replacement using the monoclinic crystal form and a mixed model of a synthetic TPR protein as search model (see Methods section). Refinement statistics are given in Table 1.

SycD structure reveals tetratricopeptide repeats

SycD behaves as a dimer in solution (see below and Ref [25]) and the monoclinic crystal form contains two molecules of $SycD_{21\text{-}163}$ per asymmetric unit. The electron density is well defined for residues 21-154 in monomer A, and for residues 21-160 in monomer B. Both monomers differ only in the position of 10 N-terminal residues indicating this region to be flexible. The rest of the molecule superposes well with an r.m.s. deviation of 1.3 Å for 125 common Cα atoms.

The SycD monomer consists of eight α-helices (h0, 1A, 1B, 2A, 2B, 3A, 3B, h8) (Figure 3a). The structure reveals the tetratricopeptide repeat (TPR)-like motifs that had been predicted for T3S class II chaperones [18]. The repeat domain in $SycD_{21\text{-}163}$ spans residues 36 to 137 and is composed of six α-helices with the helices arranged in an anti-parallel manner. The six helices 1A, 1B, 2A, 2B, 3A and 3B are organized in TPR1-3, followed by the C-terminal helix (h8) that is joined also in an antiparallel orientation resulting in 3.5 repeats overall. In a single TPR motif of SycD, helices A and B pack against each other with dihedral packing angles Ω ranging from -152 ° to -164 °, whereas packing between helices B and A' from adjoining TPR motifs show slightly lower angles (-149 ° to -158 °) as calculated by PROMOTIF [29]. The twist per repeat in the overall right-handed superhelical TPR domain of SycD is 43-49 ° between TPR1 and TPR2, 46-47 ° between TPR2 and TPR3 and 91-95 ° for the whole domain TPR1-TPR3 (rotation angles chi as obtained by superposition in LSQKAB [30]). These values are comparable with data from the literature [31]. The twisted

arrangement of the TPR motifs results in a concave and convex face of SycD (Fig 3a). The integrity of the TPR fold is maintained by a pattern of small and large residues consistent with the canonical TPR sequence motif (Trp4-Leu7-Gly8-Tyr11-Ala20-Phe24-Ala27-Pro32) [32]. The long C-terminal α–helix h8 following the TPR motifs is also termed capping, stabilization or solvating helix and is found in almost all currently known structures of TPR-containing proteins such as protein phosphatase 5 [33] and Hop [34]. A DALI search [35] for structural homologues of SycD returned Ser/Thr phosphatase 5 (PP5), the peroxisomal targeting signal receptor Pex5p, the TPR domain of CHIP U box E3 ubiquitin ligase and the O-linked N-acetylglucosaminyl transferase OGT as best matches (Z-scores 17.1, 16.2, 16.0, 15.9; r.m.s.d. 1.9, 5.0, 1.8, 1.8 Å). Taken together, the α-helical fold of class II chaperone SycD reveals genuine TPR repeats.

Comparison with the LcrH/SycD homology model discloses distinct differences

The crystal structure of $SycD_{21-163}$ monomers A and B superposes with the LcrH/$SycD_{32-165}$ homology model proposed by Pallen *et al.* [18] (PDB accession code 1OOL) showing an r.m.s. deviation of ~1.0 Å for the repeats TPR1-3 (103 equivalent Cα atoms)(not shown). However, superposition of all common residues between SycD and the model (32-160, 129 Cα atoms) increases the r.m.s. deviation to 3.6 Å, due to a completely different orientation of the C-terminal helix h8. Additional striking differences between the model and the crystal structure were observed for the side-chains of Tyr93, Phe106 and Arg71 (Figure 3b). In the model the side-chains of Tyr93 and Phe106 point outwards to the convex surface, whereas in the crystal structure both side-chains are flipped by 180 ° and deeply buried in the interstice between TPR2 and TPR3, stabilizing the TPR fold by hydrophobic interactions. Moreover, in the structure the hydroxyl group of Tyr93 points into the concave groove (Figure 3b, Figure 9c), where it may serve as hydrogen bond donor/acceptor in translocator binding. The dual

function of Tyr93 might explain the unexpected null mutant phenotype observed for LcrH Y93E [36]. Interestingly, in the crystal structure, the side-chain of Arg71 in helix A of TPR2 does not freely project into the concave groove, rather it is bent towards Glu37 from TPR1 forming an intra-molecular salt-bridge that neutralizes its positive charge (see below). To summarize, the crystal structure of SycD is similar to the LcrH homology model but discloses several differences that might help to explain observations of previous mutagenesis studies.

Ambiguity of the SycD quaternary structure

The apparent molecular mass for $SycD_{21-163}$ determined experimentally by size exclusion chromatography and dynamic light scattering gives significantly larger values (M_r ~39-42 kDa) than expected for the monomeric chaperone (~17 kDa) (compare Figure 7a), suggesting that the SycD dimer in the asymmetric unit is also present in solution. However, in the monoclinic crystal packing, different quaternary assemblies of the two SycD monomers are possible resulting in two distinct dimers (Figure 4a, b). In the elongated dimer 1, both monomers interact head-to-head via TPR1. The second assembly (dimer 2) shows the two monomers dimerizing asymmetrically back-to-back via the convex face of the TPR repeats involving TPR2 and the turns between the repeats (Figure 5).

The dimerization interfaces in dimer 1 and dimer 2 are both centered at the corresponding local rotation axis and mediated by hydrophobic interactions supported by hydrogen bonds. Dimethylated lysine Mly57 at the edge of the dimerization interface of dimer 1 supports the dimerization only via its aliphatic side-chain whereas the dimethylamino head group is not involved. Interface analyses using the PISA [37] and the protein-protein interaction server [38] (summarized in Table 2) suggested that both assemblies could result in a stable dimer. Although the structural and statistical analysis favored dimer 1, we were not able to eliminate

with certainty the alternative dimer 2. So which one is the correct SycD dimer?

SycD forms a head-to-head dimer

To verify which dimer assembly SycD adopts in solution, we mutated residues involved in the observed interfaces in order to disrupt the interaction, followed by an analysis of the mutants in solution. Based on a multiple sequence alignment of SycD and homologous TPR-containing T3S chaperones (Figure 6) we excluded highly conserved or canonical residues from mutagenesis. Concerning elongated dimer 1, we selected Ala61 and Leu65 for the mutation into large, charged glutamates (single substitutions A61E, L65E and double mutant A61E/L65E). Both residues are centrally buried in the interface and occur twice due to the 2-fold symmetry thereby facing each other (Figure 5a). The introduction of two or four negatively charged residues was expected to cause steric hindrance as well as electrostatic repulsion and, therefore, the disruption of the dimer interface. In the interface of compact dimer 2, we selected Ser94 as well as Tyr95, a key residue located at the convex surface mediating hydrophobic and hydrogen-bonded interactions between both monomers (Figure 5b). Substitution of large Tyr95 for small, polar serine instead of alanine was chosen to prevent aggregation. Equivalently to the glutamate double mutant A61E/L65E for the interface in dimer 1, we generated the double mutant S94E/Y95E for interface 2. All five $SycD_{21-163}$ mutant proteins, single site mutants A61E, L65E and Y95S as well as the double mutants A61E/L65E and S94E/Y95E, were highly soluble and could be purified in wild-type-like quantities using the same protocol as for $SycD_{21-163}$.

To investigate the oligomerization state of wild-type and mutant $SycD_{21-163}$, we performed analytical size exclusion chromatography. Wild-type $SycD_{21-163}$ as well as both dimer interface 2 mutants Y95S and S94E/Y95E elute with an apparent molecular mass of 40-43 kDa, whereas the single and double interface 1 mutants, A61E, L65E and A61E/L65E,

elute with an apparent molecular mass of ~25 kDa suggesting a monomeric species (Figure 7a). Dynamic light scattering measurements of the peak fractions gave ~38 kDa for wild-type $SycD_{21-163}$, ~40 kDa for the mutant Y95S and ~41 kDa for S95EY95E, but only ~21 kDa for mutants A61E, L65E and A61E/L65E. This is in line with the results derived from chromatography. To ensure that the effect was not caused by destroying the integrity of the TPR fold, we further analyzed the wild-type and the mutants by native PAGE and circular dichroism (CD) (wild-type and A61E/L65E, data not shown). In the native gel, $SycD_{21-163}$ wild-type and the interface mutants migrate as focused single bands consistent with folded proteins. Wild-type $SycD_{21-163}$ and the mutant Y95S (pI 5.3) migrate on the same level, whereas the single glutamate mutants A65E, L65E (pI 5.2), and more significantly the double mutants A61E/L65E and S94E/Y95E (pI_{calc} 5.1) migrate faster due to the additional surface-exposed negative charges accelerating migration in the electric field. The CD spectra of the wild-type and the mutant proteins are virtually identical displaying two minima at 208 and 222 nm that are characteristic for α-helical secondary structure elements. From these results, we concluded that the mutants were correctly folded. Dimeric mutant $SycD_{21-163}$ S94E/Y95E readily crystallized after reductive methylation, though in a different condition than wild-type $SycD_{21-163}^{meth}$ and crystals belonged to space group $P3_221$. The crystal structure of $SycD_{21-163}$ S94E/Y95E revealed a head-to-head homodimer as well, with the dimer axis being the crystallographic two-fold axis. The interfacing residues are basically the same forming a predominately hydrophobic surface (Table 2), though the two monomers are rotated more heavily with respect to each other showing a crossing angle of 90 ° instead of 61 ° as for dimer 1. This results again in an elongated though additionally kinked dimer conformation (dimer 3) that is stabilized exclusively by non-polar contacts, lacking hydrogen bonds or salt bridges between the monomers (Figure 7b). Our results from the mutational analysis and the additional mutant structure strongly suggest that the SycD dimer in solution corresponds to a head-to-head dimer and that dimerization is disrupted in the A61E, L65E and A61E/L65E

mutants.

In vivo relevance of SycD dimerization

To investigate the physiological role of SycD dimerization, we carried out *in vivo* experiments in *Yersinia* comparing a wild-type strain, a *syc*D null mutant and the *syc*D null mutant reexpressing either wild-type *syc*D or the *syc*D double mutant A61E/L65E. Culture supernatants were analyzed by SDS-PAGE to assay for Yop secretion. Total cell fractions and supernatants were analyzed by Western Blot for production and secretion of YopE and of the SycD binding partners YopB and YopD. Experiments were carried out in the absence and presence of calcium ions in order to monitor the calcium dependence of Yop production. The SycD A61E/L65E mutant showed typical characteristics of a *syc*D null mutant (Figure 8). These include the lack of YopB and YopD secretion in the absence of calcium, increased YopE production in the presence of calcium and an increased LcrV secretion independent of the calcium concentration. Mutations in the SycD dimerization interface obviously abrogate the functionality of SycD.

Implications for further interaction surfaces

To identify potential interfaces in SycD involved in protein-protein interactions, we examined the electrostatic surface potential, conserved sequence features, predicted binding sites as well as previously identified residues of SycD that are mandatory for chaperone function [22; 39; 40]. The electrostatic surface potential of the elongated dimer of $SycD_{21\text{-}163}$ is shown in Figure 9a. The flat top/bottom face of the dimer displays an extended negative charge that additionally encompasses the upper part of the concave groove, whereas the lower part of the concave face on the dimer front exposes a predominantly hydrophobic area interspersed with positively charged patches. The side-chain of Arg71 in the crystal structure is bent toward Glu37

forming a salt-bridge (compare Figure 3b) and does not create a positively charged patch on the concave face together with Arg105 contrary to the predictions derived from the homology model [18].

In addition to the region within the concave face that has been previously identified as binding groove [36], the prediction program ProMate [41] suggested a large continuous patch for protein-protein-interactions comprising additionally residues from the top of the monomer, reaching further to the upper part of the opposite, convex face (data not shown). In order to visualize the conservation of surface residues in SycD and other T3S class II chaperones and thus putative conserved interaction sites, the structure-based multiple alignment of Figure 6 was converted into a property file via ProtSkin (http://www.mcgnmr.ca/ProtSkin/). The concave surface of SycD exhibits numerous conserved amino acids, whereas the convex side of the chaperone shows little sequence conservation (Figure 9b). Most of the protein's tyrosine residues on the concave face are conserved throughout the majority of the T3S class II chaperones. Additionally conserved, surface exposed residues comprise an acidic and a heterocyclic/aromatic side-chain (Glu37, His109), as well as two leucine residues at TPR consensus positions (Leu39, Leu76) (Figure 9b,c). All of these residues line the concave groove of the chaperone with exception of Leu39 in the dimer interface, Leu76 pointing toward the convex outside and the protruding Tyr68.

Extensive random and subsequent site-directed mutational analyses complemented by investigations of mutant stability had been carried out for the binding groove, the canonical sequence motif and additional surface-exposed residues in SycD [36; 39; 40; 42], covering also most of the conserved residues mentioned above (summarized in Table 3). These studies had identified surface-located residues that are indispensable in binding to the translocators. Residues whose alanine mutants are defective in YopB- but not in YopD-binding (Phe59, Arg71, Phe72, Leu74, Gly75, His109) [39] point into the concave groove and are primarily located in TPR2 helix A (surface-located residues Arg71 and His109 depicted in Figure 9c).

Of these, Arg71 contributes to the TPR stability via a salt-bridge to conserved Glu37 (Figures 9b,c; 4c). Conserved His109 opposite in the concave groove is probably involved in YopB binding as well since mutation to alanine weakens the interaction [40] (Figure 9b and c). Thus, the concave face of SycD is most likely involved in YopB-binding. YopD binding and secretion strictly depends on His67 [39; 40] located in the turn separating TPR1 from TPR2 and Leu76, both accessible only from the convex TPR face, as well as Leu42 at the edge of the dimerization interface. Screening for suppressor mutations in the chaperone that re-established the binding to YopD mutants unable to bind wild-type LcrH disclosed additional, surface located sites involved in YopD binding, e.g. Glu30, Ile31, Leu42, His91, Asn136 [39]. Together with two additional sites associated with YopD-binding that had been identified in multiple mutants (Ile101, Lys102)[39], these residues are located on the convex face of the chaperone (Figure 9c).

Substitution of the surface exposed, conserved Tyr52 in the lower part of the concave groove has no effect albeit hydrophobic residues are preferred at this position [40]. So far uninvestigated residues near the groove are Tyr86 and the Glu37 (mentioned above), although the aromatic side-chain and the negative charge are well conserved at these positions suggesting that these two residues may be involved in the interaction with binding partners.

Alanine substitutions of conserved Tyr40 and Tyr47, exposed on the concave face, resulted in a less stable chaperone, abrogated binding and secretion of YopB and YopD and impaired the regulatory function on Yop synthesis and secretion [40], indicating that these amino acids are also necessary for maintaining the TPR integrity (Figure 9c, green). As already mentioned, conserved, buried Tyr93 with its hydroxyl group pointing into the concave groove most likely stabilizes the TPR fold, simultaneously enabling hydrogen bonds potentially required in translocator binding (Figure 4c, 9c). Residues Phe72, Phe73, Leu74, Cys79, Phe108 and Ile134 are buried and their mutation will most likely affect the TPR fold. Overall, surface-exposed residues affecting YopB binding map to the concave face of the structure whereas

those required for YopD binding are located on the convex surface (Figure 9c, red and blue). This strongly supports the idea that YopB binds to the concave face and YopD to the convex face of SycD.

Discussion

The crystal structure of SycD reveals a head-to-head dimer. This structure is the first experimental structure of a T3S class II chaperone specific for T3S translocators. It confirms the prediction that T3S class II chaperones contain TPR-like repeats and moreover shows that a structural model of the SycD monomer based on the structure of serine/threonine phosphatase 5 (PP5) [18] is in good overall agreement with the crystal structure of the SycD monomer. Under physiological conditions, however, SycD forms dimers in solution ([25], this work). Proteins containing TPR-repeats dimerize mainly via the convex outer side formed by TPR motifs in the middle of the repeat domain as observed in the crystal structures of human O-linked N-acetylglucosamine transferase (OGT) ([43], 1W3B), *P. aeruginosa* type 4 pilus protein PilF ([44], 2FI7) or the mitochondrial outer membrane transporter Tom70p ([45], 2GW1). The monomers in these dimers are tilted (in the PliF dimer by approximately 20 °). A minimal region for dimerization of the TPR domain of Hsp90 co-chaperone Sti1 has been recently identified to be located in helix A of the second TPR motif [46]. For SycD, two different assemblies of the monomers into a dimer seemed possible, based on the packing in the monoclinic crystals. The compact dimer 2 shows a back-to-back dimerization via the convex outer side, as described for other TPR-containing proteins above, exhibiting an asymmetric interface - very unusual but not unprecedented for homodimers [47; 48]. The back-to-back dimer 2 could finally be excluded by mutagenesis studies. In contrast, SycD dimerization involves mainly helices A and B of the first TPR motif generating a head-to-head assembly of a rather elongated shape with the monomers tilted by a larger angle (dimer 1 ~61).

However, the observed tailing of the size exclusion chromatography profile for SycD indicates a dimer-monomer equilibrium [49] and the stability of monomeric $SycD_{21\text{-}163}$ mutants strongly suggests that SycD dimerization is non-obligate. This is in line with the finding that SycD can form two structurally different head-to-head homodimers with distinct

arrangements of the monomers utilizing the same interface. This is extremely unusual and to the best of our knowledge, this is the first example of a homodimer exhibiting two alternative dimer assemblies sharing the same interface. SycD dimerization is almost exclusively mediated by hydrophobic contacts. There is only one hydrogen bond in the interface of dimer 1 linking the side chain of Gln60 with the backbone oxygen of Glu30. No polar interaction at all is found in dimer 3. While the hydrophobic contacts confer considerable affinity to the SycD dimer *in vitro,* the specificity may be limited, as also suggested by the two different dimer arrangements. The apparent lack of specificity implies that *in vivo* this interface could be involved in interactions other than homodimerization, e.g. localization to the membrane or the T3S apparatus, potentially via binding to so far unknown interaction partners. Known SycD binding partners include further regulatory T3S components such as TyeA and YscE [50]. SycD could possibly bind YscE via TPR motif 1 in a manner similar to that observed for the *Pseudomonas* YscE homologue PscE in complex with the TPR-like protein PscG [16].

So far, only few SycD mutations had been described that can be assigned to the dimerization interface and show an effect on translocator binding (Leu39, Leu42) [39; 40]. However, the *in vivo* phenotype of the monomeric SycD mutant A61E/L65E clearly indicates that this dimerization interface is functionally relevant. This SycD mutant is stable and folded under physiological conditions *in vitro* and both the concave and convex binding faces are intact. The null mutant-like behavior, however, suggests that either dimerization is indispensable for appropriate SycD function or that the mutation eliminated so far undetected interactions of the chaperone with the translocators or other interaction partners.

In contrast to T3S class I chaperones, where distinct features such as hydrophobic surface patches and a so-called β-motif [28] have been identified that are essential for the interaction with the specific secretion target, class II chaperones interact with multiple binding partners of different fold and function and consequentially had to develop a panoply of binding sites.

TPR-containing proteins predominantly interact with their binding partners via both the concave groove (the prevalent binding site) and the convex outer side, but basically use all possible faces of the TPR domain for ligand and inter-domain contacts (for a review see D'Andrea & Luca [51]). So far, only limited information on binding sites in class II chaperones is available, and the prediction of further interaction sites in these multivalent T3S regulators is therefore challenging.

SycD is also involved in control of effector biosynthesis by establishing a negative regulatory network on *yop* gene expression together with YopD and LcrQ (YscM1 and YscM 2 in *Y. enterocolitica*) [14; 22]. Additionally, SycD was reported to have a regulatory effect on Yop secretion via an YscY-YscX loop [52]. Regions in SycD required for YscY binding and regulatory effect were mapped to TPR1 and a so-called NEISS region located N-terminally of TPR1 with Glu30 as the key regulatory residue [22; 53]. In the crystal structure of SycD, the NEISS element is freely accessible due to its linear, exposed structure. Thus, experimental results on its regulatory role appear plausible (Figure 3, NEISS colored in magenta).

Tyrosine, an amino acid with a polar hydroxyl group, displays a high propensity to occur in protein-protein interfaces, acting as binding energy hotspot [54], and to protrude from the surface to offer suitable interaction sites [55]. Protruding tyrosines were identified to be the functional residues in a TPR-domain for binding a proline-rich ligand [56]. YopB possesses five proline residues within a short N-terminal fragment (residues 24-55). However, systematic sequence deletions in YopB did not unravel a clearly defined chaperone-binding domain. Rather several parts of the YopB sequence seem to be required for SycD binding [20].

The crystal structure of SycD and the identification of a new interaction surface in the translocator chaperone contribute to the understanding of its versatile functionality. Although both the convex as well as the concave side of the TPR in the SycD head-to-head dimer are freely accessible, stoichiometry and affinity of the SycD/YopD/YopB interactions remain to be determined. Certainly, a crystal structure of SycD in complex with one of its cognate

binding partners YopB or YopD would answer many remaining questions. However, since the translocators are hydrophobic trans-membrane proteins and can apparently bind to the chaperone in a molten globule conformation [56], such a complex structure represents a major challenge or might not be feasible at all.

Methods

Expression vector construction

Yersinia enterocolitica virulence plasmid pYVe227 (GenBank **AF102990**) served as PCR template for amplification of the *syc*D gene sequence, which was cloned into the expression vector pGEX-6P-1 (GE Healthcare) digested with restriction endonucleases BamHI and EcoRI. A second construct was generated by cloning codons 21-163 of *syc*D into the same vector. Both constructs were checked by sequencing.

Protein expression and purification

E. coli BL21(DE3) codon plus RIL (Stratagene) was used to produce full-length SycD and $SycD_{21-163}$ as GST-fusion proteins. Cultures were grown at 37 °C to an OD_{600} of 0.9. Recombinant gene expression was induced with 0.25 mM isopropyl-β-D-thiogalactoside at 20 °C for 14 h. Cells were resuspended in ice-cold lysis buffer (phosphate buffered saline (PBS) /10 mM β-mercaptoethanol (βME) /5 µL Benzonase (MERCK) /protease inhibitor cocktail (Roche), pH 7.4) and lysed using a homogenizer (Constant Cell Disruption Systems). Cleared lysates were applied to glutathione-coupled sepharose resin (GE Healthcare) and washed with lysis buffer, finally with protease cleavage buffer (50 mM Tris /150 mM NaCl /10 mM βME /1 mM EDTA, pH 7.4). The GST-tag was cleaved on column at 4 °C over 48-60 h adding 500 U PreScission Protease (GE Healthcare). The PreScission cleavage site inserts five additional residues (Gly-Pro-Leu-Gly-Ser, assigned as -5 to -1) at the N-terminus. The supernatant was dialyzed against 50 mM Tris-HCl, pH 8.0, 5 mM DTT.

SycD and $SycD_{21-163}$ were further purified by anion exchange chromatography (MonoQ, GE Healthcare) using a NaCl gradient in 50 mM Tris-HCl, pH 8.0. Size exclusion chromatography (Superdex 200, GE Healthcare) in 10 mM Tris pH 8.0, 50 mM NaCl, 1 mM DTT as running buffer was used as the final purification step. Purified protein was analyzed

by native as well as SDS-PAGE, subjected to MALDI-TOF analysis to verify the protein size and concentrated to 14 mg/mL ($SycD_{21\text{-}163}^{meth}$) and 23 mg/mL ($SycD_{21\text{-}163}$) for crystallization trials.

Limited proteolysis and reductive methylation

Purified full-length SycD (0.8 mg/mL) was digested at 20 °C with 1:100 trypsin (seq. grade, modified, Promega) and aliquots were taken during the reaction course. Digestion products were separated by SDS-PAGE, blotted onto PVDF membrane and analyzed by N-terminal sequencing.

$SycD_{21\text{-}163}$ purified by anion exchange chromatography was subjected to ultrafiltration using Vivaspin 20 (Sartorius, MWCO 5'000) for buffer exchange with 50 mM sodium potassium phosphate /150 mM NaCl, pH 7.5. The protein was concentrated to ~10 mg/mL in a total volume of 2*1 mL and methylated as described [57]. Briefly, 1 mL protein solution was gently mixed with 20 µL of 1 M dimethylamine-borane complex (ABC) immediately followed by the addition of 40 µL of 1 M formaldehyde and incubated on ice and in the dark for 2 h. The reaction step was repeated twice with only half of the volumes added in the third round followed by incubation for 36 h. Quenching of the reaction was achieved by addition of 100 µL of 1 M ammonium sulfate and incubation for 24 h. The methylated protein was mixed with 50 mM DTT to a final concentration of 5 mM and separated from reaction residue by size exclusion chromatography as described above.

Molecular mass determination

Size exclusion chromatography was carried out using a Superdex 200 HR 10/30 column pre-equilibrated in 10 mM Tris pH 8.0 /150 mM NaCl /1 mM DTT (protein loading 0.66 -

3.9 mg/mL) calibrated with low and high molecular mass standard proteins (GE Healthcare). Dynamic light scattering was performed in a DynaPro 801TC system (ProteinSolutions, sample concentrations 0.8 - 5.4 mg/mL).

Crystallization, data collection and processing

Initial screening for $SycD_{21-163}$ in 96-well format using diverse commercially available crystallization matrices and nanoliter pipetting yielded tiny needles. Optimized tetragonal $SycD_{21-163}$ crystals grew within two weeks at 4 °C using hanging drop vapor diffusion by adding 0.4 µL of crystallization cocktail (1.9-2.2 potassium acetate /0.1 M Tris pH 8.2) to 2 µL protein solution. Extensive initial screening for reductively methylated $SycD_{21-163}^{meth}$ produced crystalline plates in a single condition at 4 °C. Optimized monoclinic crystals of $SycD_{21-163}^{meth}$ grew in 10-20 % 2-propanol, 20-23 % polyethylene glycol 4'000 and 0.1 M sodium acetate using sitting drop vapor diffusion and a protein:reservoir ratio of 2:1. Initial, well diffracting crystals of reductively methylated $SycD_{21-163}$ S94E/Y95E formed within three days at 4 °C from a crystallization cocktail containing 40 % PEG400, 5 % PEG 3'350 and 0.1 M sodium acetate pH 5.5.

Data of $SycD_{21-163}$ and $SycD_{21-163}^{meth}$ were collected at 100 K using 20-26 % glycerol in the crystallization mix as cryoprotectant at beamlines DESY/EMBL X12 (Hamburg, Germany) and ESRF ID23-1 (Grenoble, France). Data of $SycD_{21-163}$ S94E/Y95E ^{meth} crystals flash-frozen without additional cryo-protectant were collected at beamline ESRF ID14-1. Data of $SycD_{21-163}$ were processed with HKL2000 (DENZO/SCALEPACK) [58]. Data of $SycD_{21-163}^{meth}$ and $SycD_{21-163}$ S94E/Y95E^{meth} were processed with XDS and scaled with XSCALE [59]. Data collection statistics are given in Table 1.

Structure determination and analysis

The structure for the monoclinic data set of $SycD_{21\text{-}163}^{meth}$ was solved by molecular replacement (MR) in the program PHASER [60]. Correct localization of both monomers in the asymmetric unit was only achieved by searching with a mixed model of the TPR domain of a synthetic protein (PDB accession code 2FO7), obtained by application of the Fold and Function Assignment System (FFAS) algorithm to the SycD sequence [61]. The correct MR solution became evident only after placing the second monomer in PHASER. The initial 68 % complete model was refined using the rigid body and simulated annealing tools of the program suite PHENIX [62]. The final model was obtained by several cycles of manual building with the program COOT [63] and restrained refinement with REFMAC5[64] or PHENIX. The refined model was later used for MR of $SycD_{21\text{-}163}$ S94E/Y95E^{meth}. Electron density was visible for $SycD_{21\text{-}163}^{meth}$ residues 21-154 in the first monomer, and residues 21-160 in the second. For $SycD_{21\text{-}163}$ S94E/Y95E^{meth}, electron density was visible for residues 29-160 only. A composite omit map was calculated with CNS [65]. Protein interfaces and quaternary structures were identified using PISA [37], the protein-protein interaction server (http:// www.biochem.ucl.ac.uk/ bsm/ PP/ server/) [38] and ProMate [41]. Ribbon diagrams and surfaces were produced with PyMOL [66], secondary structure assignment was calculated using STRIDE [67]. Pairwise and multiple sequence alignments were produced with EMBOSS [68] and CLUSTALW [69] and visualized with ESPRIPT [70]. Structures were aligned with DALI [35] and LSQKAB [30].

In vivo experiments

SycD wild-type and mutant A61E/L65E sequences were cloned into the NcoI/EcoRI sites of pBADmycHisA (silent mutation of the internal *syc*D NcoI site) giving plasmids pISO156 and pISO157. Induction of the *yop* regulon was described by Cornelis *et al.*[71]. The bacteria were

cultivated in permissive (Brain-heart infusion, BHI, supplemented with 20 mM sodium oxalate (-Ca^{2+})) or non-permissive conditions (BHI supplemented with 5 mM calcium chloride (+Ca^{2+})) [71; 72]. Expression of the different genes cloned downstream from the pBAD promoter was routinely induced by adding 0.2 % L-arabinose to the culture just before the shift to 37 °C, and again 2 h later. The carbon source was glycerol (4 mg/ml). Total cell and supernatant fractions were separated by centrifugation at 20'800xg for 10 min at 4 °C. The cell pellet was taken as total cell fraction. Proteins in the supernatant were precipitated using trichloroacetic acid 10 % (w/v) final for 1 h at 4 °C.

Secreted proteins were analyzed on Coomassie-stained 12 % SDS-PAGE. In each case proteins secreted by $3x10^8$ bacteria were loaded per lane. For detection of proteins by immunoblotting, $1.6x10^8$ bacteria (total cell fraction) and supernatants from $2.5x10^7$ bacteria (supernatant fraction) were loaded per lane. Immunoblotting was carried out using polyclonal rat-antibodies directed against YopB (MIPA98; 1:300), YopD (MIPA96; 1:300) and YopE (MIPA94; 1:10'000) or polyclonal rabbit-antibodies directed against SycD (MIPA35; 1:1'000). Detection was performed with the respective secondary antibodies conjugated to horseradish peroxidase (1:5'000; Dako) before development with supersignal chemiluminescent substrate (Pierce).

Coordinates

Coordinates and structure factors have been deposited in the Protein Data Bank (accession codes 2vgx, 2vgy).

Acknowledgements

We are grateful to Dr. Axel Scheidig and Dr. Yvonne Carius for data collection at ESRF ID23-1, and to Dr. Manfred Weiss and Dr. Santosh Panjikar (DESY/EMBL, beamline X12) for help with xenon derivatization, data collection and processing. We thank Rita Getzlaff for N-terminal sequencing and Dr. Manfred Nimtz and Anja Meier for MALDI-TOF measurements. This work was supported by the DFG priority program 1150 - "Signaling pathways to the cytoskeleton and bacterial pathogenicity" (to H.H.N.) and the Fonds der Chemischen Industrie (to D.W.H.).

References

1. Mota, L. J. & Cornelis, G. R. The bacterial injection kit: type III secretion systems. *Ann. Med.* **37** (2005), pp. 234-249.
2. Navarro, L., Alto, N. M. & Dixon, J. E. Functions of the *Yersinia* effector proteins in inhibiting host immune responses. *Curr. Opin. Microbiol.* **8** (2005), pp. 21-27.
3. Galan, J. E. & Wolf-Watz, H. Protein delivery into eukaryotic cells by type III secretion machines. *Nature* **444** (2006), pp. 567-573.
4. Büttner, D. & Bonas, U. Port of entry - the type III secretion translocon. *Trends Microbiol.* **10** (2002), pp. 186-192.
5. Parsot, C., Hamiaux, C. & Page, A.-L. The various and varying roles of specific chaperones in type III secretion systems. *Curr. Opin. Microbiol.* **6** (2003), pp. 7-14.
6. Feldman, M. F. & Cornelis, G. R. The multitalented type III chaperones: all you can do with 15 kDa. *FEMS Microbiol. Lett.* **219** (2003), pp. 151-158.
7. Wilharm, G., Dittmann, S., Schmid, A. & Heesemann, J. On the role of specific chaperones, the specific ATPase, and the proton motive force in type III secretion. *Int. J. Med. Microbiol.* **297** (2007), pp. 27-36.
8. Letzelter, M., Sorg, I., Mota, L. J., Meyer, S., Stalder, J., Feldman, M., Kuhn, M., Callebaut, I. & Cornelis, G. R. The discovery of SycO highlights a new function for type III secretion effector chaperones. *EMBO J.* **25** (2006), pp. 3223-3233.
9. Luo, Y., Bertero, M. G., Frey, E. A., Pfuetzner, R. A., Wenk, M. R., Creagh, L., Kay, C., Haynes, C., Finley, B. B. & Strydnaka, N. C. J. Structural and biochemical characterization of the type III secretion chaperones CesT and SigE. *Nat. Struct. Biol.* **8** (2001), pp. 1031-1036.
10. Thomas, J., Stafford, G. P. & Hughes, C. Docking of cytosolic chaperone-substrate complexes at the membrane ATPase during flagellar type III protein export. *PNAS* **101** (2004), pp. 3945-3950.
11. Wulff-Strobel, C. R., Williams, A. W. & Straley, S. C. LcrQ and SycH function together at the Ysc type III secretion system in *Yersinia pestis* to impose a hierarchy of secretion. *Mol.*

Microbiol. **43** (2002), pp. 411-423.

12. Darwin, K. H. & Miller, V. L. Type III secretion chaperone-dependent regulation: activation of virulence genes by SicA and InvF in *Salmonella typhimurium*. *EMBO J.* **20** (2001), pp. 1850-1862.

13. Mavris, M., Page, A.-L., Tournebize, R., Demers, B., Sansonetti, P. & Parsot, C. Regulation of transcription by the activity of the *Shigella flexneri* type III secretion apparatus. *Mol. Microbiol.* **43** (2002), pp. 1543-1553.

14. Anderson, D. M., Ramamurthi, K. S., Tam, C. & Schneewind, O. YopD and LcrH regulate expression of *Yersinia enterocolitica* YopQ by a posttranscriptional mechanism and bind to yopQ RNA. *J. Bacteriol.* **184** (2002), pp. 1287-1295.

15. Johnson, S., Deane, J. E. & Lea, S. M. The type III needle and the damage done. *Curr. Opin. Struct. Biol.* **15** (2005), pp. 700-707.

16. Quinaud, M., Ple, S., Job, V., Contreras-Martel, C., Simorre, J.-P., Attree, I. & Dessen, A. Structure of the heterotrimeric complex that regulates type III secretion needle formation. *PNAS* **104** (2007), pp. 7803-7808.

17. Yip, C. K., Finlay, B. B. & Strynadka, N. C. J. Structural characterization of a type III secretion system filament protein in complex with its chaperone. *Nat. Struct. Mol. Biol.* **12** (2005), pp. 75-81.

18. Pallen, M. J., Francis, M. S. & Futterer, K. Tetratricopeptide-like repeats in type-III-secretion chaperones and regulators. *FEMS Microbiol. Lett.* **223** (2003), pp. 53-60.

19. Wattiau, P., Bernier, B., Deslee, P., Michiels, T. & Cornelis, G. R. Individual chaperones required for Yop secretion by *Yersinia*. *PNAS* **91** (1994), pp. 10493-10497.

20. Neyt, C. & Cornelis, G. R. Role of SycD, the chaperone of the *Yersinia* Yop translocators YopB and YopD. *Mol. Microbiol.* **31** (1999), pp. 143-156.

21. Day, J. B. & Plano, G. V. The *Yersinia pestis* YscY Protein Directly Binds YscX, a Secreted Component of the Type III Secretion Machinery. *J. Bacteriol.* **182** (2000), pp. 1834-1843.

22. Francis, M. S., Lloyd , S. A. & Wolf-Watz, H. The type III secretion chaperone LcrH co-operates with YopD to establish a negative, regulatory loop for control of Yop synthesis in

Yersinia pseudotuberculosis. *Mol. Microbiol.* **42** (2001), pp. 1075-1093.

23. Cambronne, E. D., Sorg, J. A. & Schneewind, O. Binding of SycH chaperone to YscM1 and YscM2 activates effector yop expression in *Yersinia enterocolitica*. *J. Bacteriol.* **186** (2004), pp. 829-841.

24. Tengel, T., Sethson, I. & Francis, M. S. Conformational analysis by CD and NMR spectroscopy of a peptide encompassing the amphipathic domain of YopD from *Yersinia*. *Eur. J. Biochem.* **269** (2002), pp. 3659-3668.

25. Schmid, A., Dittmann, S., Grimminger, V., Walter, S., Heesemann, J. & Wilharm, G. *Yersinia enterocolitica* type III secretion chaperone SycD: recombinant expression, purification and characterization of a homodimer. *Protein Expr. Purif.* **49** (2006), pp. 176-182.

26. Matthews, B. W. Solvent content of protein crystals. *J. Mol. Biol.* **33** (1968), pp. 491-497.

27. Schubot, F. D. & Waugh, D. S. A pivotal role for reductive methylation in the de novo crystallization of a ternary complex composed of *Yersinia pestis* virulence factors YopN, SycN and YscB. *Acta Cryst. D* **60** (2004), pp. 1981-1986.

28. Lilic, M., Vujanac, M. & Stebbins, C. E. A Common Structural Motif in the Binding of Virulence Factors to Bacterial Secretion Chaperones. *Mol. Cell* **21** (2006), pp. 653-664.

29. Hutchinson, E. G. & Thornton, J. M. PROMOTIF--a program to identify and analyze structural motifs in proteins. *Protein Sci.* **5** (1996), pp. 212-220.

30. Kabsch, W. A solution for the best rotation to relate two sets of vectors. *Acta Cryst. A* **32** (1976), pp. 922-923.

31. Main, E. R., Xiong, Y., Cocco, M. J., D'Andrea, L. & Regan, L. Design of stable alpha-helical arrays from an idealized TPR motif. *Structure* **11** (2003), pp. 497-508.

32. Sikorski, R. S., Boguski, M. S., Goebl, M. & Hieter, P. A repeating amino acid motif in CDC23 defines a family of proteins and a new relationship among genes required for mitosis and RNA synthesis. *Cell* **60** (1990), pp. 307-317.

33. Das, A. K., Cohen, P. W. & Barford, D. The structure of the tetratricopeptide repeats of protein phosphatase 5: implications for TPR-mediated protein-protein interactions. *EMBO J.* **17** (1998), pp. 1192-1199.

34. Scheufler, C., Brinker, A., Bourenkov, G., Pegoraro, S., Moroder, L., Bartunik, H., Hartl, F. U. & Moarefi, I. Structure of TPR domain-peptide complexes: Critical elements in the assembly of the Hsp70-Hsp90 multichaperone machine. *Cell* **101** (2000), pp. 199-210.

35. Holm, L., Sander, C. Protein Structure Comparison by Alignment of Distance Matrices. *J. Mol. Biol.* **233** (1993), pp. 123-138.

36. Broms, J. E., Edqvist, P. J., Forsberg, A. & Francis, M. S. Tetratricopeptide repeats are essential for PcrH chaperone function in *Pseudomonas aeruginosa* type III secretion. *FEMS Microbiol. Lett.* **256** (2006), pp. 57-66.

37. Krissinel, E. & Henrick, K. Detection of protein assemblies in crystals. *Lect Notes Comput Sc* **3695** (2005), pp. 163-174.

38. Laskowski, R. A. SURFNET: a program for visualizing molecular surfaces, cavities, and intermolecular interactions. *Journal of molecular graphics* **13** (1995), pp. 323-330, 307-328.

39. Francis, M. S., Aili, M., Wiklund, M.-L. & Wolf-Watz, H. A study of the YopD-LcrH interaction from *Yersinia pseudotuberculosis* reveals a role for hydrophobic residues within the amphipathic domain of YopD. *Mol. Microbiol.* **38** (2000), pp. 85-102.

40. Edqvist, P. J., Broms, J. E., Betts, H. J., Forsberg, A., Pallen, M. J. & Francis, M. S. Tetratricopeptide repeats in the type III secretion chaperone, LcrH: their role in substrate binding and secretion. *Mol. Microbiol.* **59** (2006), pp. 31-44.

41. Neuvirth, H., Raz, R. & Schreiber, G. ProMate: A Structure Based Prediction Program to Identify the Location of Protein-Protein Binding Sites. *J. Mol. Biol.* **338** (2004), pp. 181-199.

42. Edqvist, P. J., Aili, M., Liu, J. & Francis, M. S. Minimal YopB and YopD translocator secretion by *Yersinia* is sufficient for Yop-effector delivery into target cells. *Microbes Infect.* **9** (2007), pp. 224-233.

43. Jinek, M., Rehwinkel, J., Lazarus, B. D., Izaurralde, E., Hanover, J. A. & Conti, E. The superhelical TPR-repeat domain of O-linked GlcNAc transferase exhibits structural similarities to importin alpha. *Nat. Struct. Mol. Biol.* **11** (2004), pp. 1001-1007.

44. Kim, K., Oh, J., Han, D., Kim, E. E., Lee, B. & Kim, Y. Crystal structure of PilF: Functional implication in the type 4 pilus biogenesis in *Pseudomonas aeruginosa*. *Biochem. Biophys. Res.*

Commun. **340** (2006), pp. 1028-1038.

45. Wu, Y. & Sha, B. Crystal structure of yeast mitochondrial outer membrane translocon member Tom70p. *Nat. Struct. Mol. Biol.* **13** (2006), pp. 589-593.

46. Flom, G., Behal, R. H., Rosen, L., Cole, D. G. & Johnson, J. L. Definition of the minimal fragments of Sti1 required for dimerization, interaction with Hsp70 and Hsp90 and in vivo functions. *Biochem. J.* (2007).

47. Cha, H., Kopetzki, E., Huber, R., Lanzendorfer, M. & Brandstetter, H. Structural Basis of the Adaptive Molecular Recognition by MMP9. *J. Mol. Biol.* **320** (2002), pp. 1065-1079.

48. Deo, R. C., Groft, C. M., Rajashankar, K. R. & Burley, S. K. Recognition of the Rotavirus mRNA 3' Consensus by an Asymmetric NSP3 Homodimer. *Cell* **108** (2002), pp. 71-81.

49. Yu, C.-M., Mun, S. & Wang, N.-H. L. Theoretical analysis of the effects of reversible dimerization in size exclusion chromatography. *Journal of Chromatography A* **1132** (2006), pp. 99-108.

50. Swietnicki, W., O'Brien, S., Holman, K., Cherry, S., Brueggemann, E., Tropea, J. E., Hines, H. B., Waugh, D. S. & Ulrich, R. G. Novel protein-protein interactions of the *Yersinia pestis* type III secretion system elucidated with a matrix analysis by surface plasmon resonance and mass spectrometry. *J. Biol. Chem.* **279** (2004), pp. 38693-38700.

51. D'Andrea, L. D. & Regan, L. TPR proteins: the versatile helix. *Trends Biochem. Sci.* **28** (2003), pp. 655-662.

52. Iriarte, M. & Cornelis, G. R. Identification of SycN, YscX, and YscY, three new elements of the *Yersinia* Yop virulon. *J. Bacteriol.* **181** (1999), pp. 675-680.

53. Broms, J. E., Edqvist, P. J., Carlsson, K. E., Forsberg, A. & Francis, M. S. Mapping of a YscY binding domain within the LcrH chaperone that is required for regulation of *Yersinia* type III secretion. *J. Bacteriol.* **187** (2005), pp. 7738-7752.

54. Bogan, A. A. & Thorn, K. S. Anatomy of hot spots in protein interfaces. *J. Mol. Biol.* **280** (1998), pp. 1-9.

55. Jones, S. & Thornton, J. M. Protein-protein interactions: A review of protein dimer structures. *Prog. Biophys. Mol. Biol.* **63** (1995), pp. 31-59.

56. Faudry, E., Job, V., Dessen, A., Attree, I. & Forge, V. Type III secretion system translocator has a molten globule conformation both in its free and chaperone-bound forms. *FEBS Journal* **274** (2007), pp. 3601-3610.

57. Rypniewski, W. R., Holden, H. M. & Rayment, I. Structural consequences of reductive methylation of lysine residues in hen egg white lysozyme: an X-ray analysis at 1.8-A resolution. *Biochemistry* **32** (1993), pp. 9851-9858.

58. Otwinowski, Z., Minor, W. Processing of X-ray difraction data collected in oscillation mode. *Methods Enzymol.* **276** (1997), pp. 307-326.

59. Kabsch, W. Automatic processing of rotation diffraction data from crystals of initially unknown symmetry and cell constants. *J. Appl. Cryst.* **26** (1993), pp. 795-800.

60. Storoni, L. C., McCoy, A. J. & Read, R. J. Likelihood-enhanced fast rotation functions. *Acta Cryst. D* **60** (2004), pp. 432-438.

61. Rychlewski, L., Jaroszewski, L., Li, W. & Godzik, A. Comparison of sequence profiles. Strategies for structural predictions using sequence information. *Protein Sci.* **9** (2000), pp. 232-241.

62. Adams, P. D., Grosse-Kunstleve, R. W., Hung, L.-W., Ioerger, T. R., McCoy, A. J., Moriarty, N. W., Read, R. J., Sacchettini, J. C., Sauter, N. K. & Terwilliger, T. C. PHENIX: building new software for automated crystallographic structure determination. *Acta Cryst. D* **58** (2002), pp. 1948-1954.

63. Emsley, P. & Cowtan, K. Coot: model-building tools for molecular graphics. *Acta Cryst. D* **60** (2004), pp. 2126-2132.

64. Murshudov, G. N., Vagin, A. A., Dodson, E. J. Refinement of macromolecular structures by the maximum-likelihood method. *Acta Cryst. D* **53** (1997), pp. 240-255.

65. Brunger, A. T., Adams, P. D., Clore, G. M., DeLano, W. L., Gros, P., Grosse-Kunstleve, R. W., Jiang, J. S., Kuszewski, J., Nilges, M., Pannu, N. S., Read, R. J., Rice, L. M., Simonson, T. & Warren, G. L. Crystallography & NMR system: A new software suite for macromolecular structure determination. *Acta Cryst. D* **54** (1998), pp. 905-921.

66. DeLano, W. L. *The PyMOL Molecular Graphics System* (2002), DeLano Scientific, San

Carlos, CA, USA.

67. Heinig, M. & Frishman, D. STRIDE: a web server for secondary structure assignment from known atomic coordinates of proteins. *Nucl. Acids. Res.* **32** (2004), pp. W500-502.

68. Pearson, W. R., Wood, T., Zhang, Z. & Miller, W. Comparison of DNA sequences with protein sequences. *Genomics* **46** (1997), pp. 24-36.

69. Thompson, J. D., Higgins, D. G., Gibson, T. J. CLUSTAL W: improving the sensitivity of progressive multiple sequence alignment through sequence weighting, position-specific gap penalties and weight matrix choice. *Nucl. Acids. Res.* **22** (1994), pp. 4673-4680.

70. Gouet, P., Courcelle, E., Stuart, D. I. & Metoz, F. ESPript: analysis of multiple sequence alignments in PostScript. *Bioinformatics* **15** (1999), pp. 305-308.

71. Cornelis, G., Vanootegem, J. C. & Sluiters, C. Transcription of the yop regulon from Y. enterocolitica requires trans acting pYV and chromosomal genes. *Microb Pathog* **2** (1987), pp. 367-379.

72. Marenne, M. N., Journet, L., Mota, L. J. & Cornelis, G. R. Genetic analysis of the formation of the Ysc-Yop translocation pore in macrophages by Yersinia enterocolitica: role of LcrV, YscF and YopN. *Microb Pathog* **35** (2003), pp. 243-258.

73. Baker, N. A., Sept, D., Joseph, S., Holst, M. J. & McCammon, J. A. Electrostatics of nanosystems: application to microtubules and the ribosome. *PNAS* **98** (2001), pp. 10037-10041.

74. Diederichs, K. & Karplus, P. A. Improved R-factors for diffraction data analysis in macromolecular crystallography. *Nat. Struct. Biol.* **4** (1997), pp. 269-275.

75. Lawrence, M. C. & Colman, P. M. Shape complementarity at protein/protein interfaces. *J. Mol. Biol.* **234** (1993), pp. 946-950.

Figures

Figure 1.

SDS-PAGE analysis of limited proteolysis of full-length SycD. The tryptic digest at 20 °C resulted in a stable fragment of SycD that is N-terminally truncated by 20 amino acids.

Figure 2.

a) MALDI-TOF mass spectrum of reductively methylated $SycD_{21-163}$. [M+H] indicates the singly-charged species, [M+2H] the doubly-charged ion. Molecular mass for $SycD_{21-163}^{meth}$ calculated from amino acid sequence with complete dimethylation of 10 lysines and the N-terminus is 16'794 Da.

b) Composite omit map of electron density contoured at 1.0 σ for dimethylated residue Lys51 (Mly51, green) involved in a crystal contact, 2Fo - Fc Fourier map at 1.0 σ for remaining residues. Five out of 10 lysine side-chains per monomer, Lys51, Lys57, Lys102, Lys117 and Lys137, were well defined in electron density.

Figure 3

a) Stereo image of the crystal structure of monomeric $SycD_{21-163}$. Front view of the concave side and top view after turning by 90 °, with TPR1 in yellow , TPR2 in green and TPR3 in blue. 'A' helices are pastel-colored. The C-terminal stabilization helix h8 is colored in red. b) Stereo close-up view of $SycD_{21-163}$ (blue, side chains as yellow sticks) superposed onto the LcrH/SycD homology model [18] (light grey, brown) revealing side-chain deviations for Tyr93, Phe106 and Arg71.

Figure 4

Alternative homodimer assemblies of $SycD_{21\text{-}163}$. a) Monoclinic crystal packing of SycD allows two different dimer assemblies. Elongated dimer 1 is composed of the blue and yellow monomer, compact dimer 2 of the blue and orange monomer. b) Ribbon diagram of dimer 1 and dimer 2 with the monomers colored in blue and yellow. View along the two-fold rotation axis in dimer 1 with the monomers tilted by ~61 °. Dimer 2 is asymmetric. View perpendicular to the imperfect two-fold rotation axis. Interface sections are indicated by dashed lines.

Figure 5

Stereo views of the dimerization interface in dimer 1 (a) and dimer 2 (b), respectively. Residues chosen for mutational analysis are highlighted in red. Hydrogen bonds are depicted as green dashed lines.

Figure 6

Structure-based alignment of T3S class II chaperones, generated with ESPript. *Y. enterocolitica* SycD (GenBank accession numbers **AAD16814**), *P. aeruginosa* PcrH (**NP250398**), *E. coli* CesD (**AAC38376**), *Salmonella typhimurium* SicA (**AAB06794)**, *Shigella flexneri* IpgC (**P0A2U4**), *Chlamydia trachomatis* LcrH-1 (**NP220091**), *Burkholderia pseudomallei* BicA (**YP335732**), *Y. enterocolitica* SycB (**AAM47500**), *S. typhimurium* SscB (**NP460368**) and SscA (**NP460364**). -TPR1, ≡ TPR2, = TPR3. • Canonical residues at TPR positions 8, 20, 27, **o** conserved residues at positions 4, 7, 11, 24, 32. Interfacing residues are shaded blue. For purposes of clarity only the first five sequences are depicted. Conserved surface residues, as derived from ProtSkin (see main text and Figure 9b) by analysis of the complete alignment, are highlighted in orange.

Figure 7

a) Analytical size exclusion chromatography of wild-type $SycD_{21-163}$ (black curve, 3) and $SycD_{21-163}$ dimer interface mutants S94E/Y95E (light orange, 1), Y95S (orange, 2), A61E/L65E (light grey, 4), L65E (grey, 5) and A61E (dark blue, 6). Loading concentrations 0.6-3.9 mg/mL. Apparent molecular masses obtained for 1: ~ 43 kDa, 2 and 3: ~40 kDa, 4, 5 and 6: ~ 25 kDa. Theoretical mass of monomeric wild-type $SycD_{21-163}$ ~16.5 kDa. b) Crystal structure of the $SycD_{21-163}$ S94E/Y95E ^{meth} head-to-head dimer. Views perpendicular to and along the two-fold rotational crystallographic symmetry axis. The 90 ° crossing angle between the monomers results in an kinked, alternative dimer assembly (dimer 3).

Figure 8

In vivo relevance of the SycD dimerization interface. Yop expression and secretion of *Yersinia* in the absence and presence of Ca^{2+}, detected by (a) Coomassie-stained SDS-PAGE of the culture supernatant and (b) Western blot of total cell and supernatant fractions. *Yersinia* wild-type, a *syc*D knockout Δ*syc*D, and Δ*syc*D reexpressing either wild-type *syc*D or the monomeric A61E/L65E mutant (*syc*D*). The A61E/L65E mutant shows a null mutant-like phenotype. Note: The polyclonal antibody against SycD cross-reacts with a band (marked with a cross) running directly below SycD.

Figure 9

Surface representation of $SycD_{21-163}$ monomer and dimer. a) The electrostatic surface potential of the elongated $SycD_{21-163}$ homodimer was calculated using the APBS [73] plug-in of PyMOL. The dimer surface exposing both concave TPR faces harbors positively charged patches. A negatively charged patch is located on the flat dimer top/bottom face (after a 90 ° turn upwards). b) Sequence conservation drawing for the $SycD_{21-163}$ monomer as obtained by

ProtSkin (http://www.mcgnmr.ca/ProtSkin/). Orange denotes conserved regions. Tyrosines are highly conserved and line the inner groove. The convex side shows only minimal conservation. c) Key residues located at the surface of $SycD_{21-163}$ that are involved in YopD secretion (dark blue: single mutations; light blue: likely involved, multiple mutations) and YopB binding and secretion (red) (see references [39; 40]). Residues accompanied by a non-binding and non-secreting phenotype (Tyr40, Tyr47, Tyr93; see reference above) are colored green.

Table 1. Data collection and refinement statistics.

	$SycD_{21-163}$	$SycD_{21-163}^{meth}$	$SycD_{21-163}^{meth}$ S94E/Y95E
Data collection statistics			
Beamline	ESRF ID23-1	ESRF ID23-1	ESRF ID14-1
Space group	$P4_122$ / $P4_322$	C2	$P3_221$
Unit cell dimensions [Å], [°]	a=b= 211.6, c= 242.5, α=β=γ= 90	a= 107.3 b= 33.0, c= 96.7, α = γ = 90 β= 122.3	a=b= 90.6, c= 54.2, α=β=90 γ= 120
Wavelength [Å]	1.2781	0.979250	0.934
Resolution [Å]	50-3.85 (3.99-3.85)	45-1.95 (2.05-1.95)	39-2.6 (2.7-2.6)
Mosaicity [°]	0.3	0.32	0.315
Completeness [%]	99.9 (99.9)	99.6 (99.8)	99.6 (100.0)
Redundancy	7.8	4	7.2
Observations	412632	84992	58856
Unique reflections	53183	21282	8163
I/σ(I)	12.0 (3.0)	13.1 (3.8)	20 (3.7)
Rsym [a], Rmeas [b]	17.2 (75.2)	9.5 (40.6)	10.5 (56.2)
Phasing	-	Mol. Replacement	Mol. Replacement
Molecules per asymm. unit	approx. 34	2	1
Solvent content [%]	49	43	68
Refinement statistics			
R / R_{free} [c] [%]		17.5 / 22.6	21.3 / 23.4
Atoms Protein/Solvent		2343 / 137	1069 / 28
R.m.s. deviation			Mean deviation
Bonds [Å] /Angles [°]		0.017 / 1.455	0.006 / 0.806
Ramachandran Plot			
Residues in allowed / additionally / generously allowed regions [%]		93.5 / 6.5 / 0.0	90.0 / 10.0 / 0.0
Residues in disallowed regions [%]		0	0
B factor [Å^2] average / Wilson B	- / 81.4	19.9 / 22.1	55.5 / 49.6
Protein / Solvent		18.4 / 30.0	54.4 / 52.8

Values in parentheses are for the highest resolution shell.

[a] $R_{sym} = 100\ \Sigma_n\ (\Sigma_i\ |I_i - \hat{I}|)/\ \Sigma_n\ (\Sigma I_i)$

[b] $R_{meas} = 100\ n\ \Sigma_I\ |\hat{I} - I_i|/\Sigma_{hkl}\ (n-1)\ \Sigma_i I_i$, where $\hat{I}$ is the mean intensity of symmetry-related reflections [74].

[c] $R = 100\ \Sigma_{hkl}\ |F_{obs} - F_{calc}|\ \Sigma_{hkl}\ F_{obs}$. Test set size 5 %.

Table 2. SycD dimer interface statistics.

Interface statistics	Dimer (1) elongated	Dimer (2) compact	Dimer (3) kinked
Monomer buried SA [Å^2]	924	655	607
% Monomer SA	11.0	7.8	7.5
Number of residues	25	18	21
% Non-polar atoms [a]	72.6	78.7	68.7
% Polar atoms [a]	27.6	22.8	31.3
Planarity [a]	2.3	1.9	2.9
Hydrogen bonds	2	3	0
Salt bridges	0	0	0
Gap volume index [a]	2.03	4.07	3.84
Shape correlation statistics [b]	0.617	0.699	0.548

Values were obtained with PISA, [a] calculated by Protein-Protein Interaction server, [b] calculated by SC [75].

Table 3. Correlation of previous mutagenesis [39; 40] results with the SycD crystal structure.

Residue/Mutation	Binding/Secretion/ Stability	Structure
H67*A	- / D↓ / WT	Turn, convex face
L42*A	- / D↓ / WT	Dimerization interface
L76*A	- / D↓ / ↓	Accessible from convex face, fold (?)
E30G, I31V, L42*F, H91Y, D136G	Suppressor mutations D↑	Loops, convex face, dimeriz. interface
I101*M, K102R	D↓ / n.d./ n.d.	Turn, convex face
R71A	D B↓ / B↓ / ↓	Salt-bridge to Glu37
H109A (as double mutant F108A)	D B↓ / B↓ / ↓	Concave face
Glu37	n.d. / n.d. / n.d.	Concave, salt-bridge to Arg71
Y52A	WT / WT / WT	Concave face
Tyr86	n.d. / n.d. / n.d.	Concave face
L39A	n.d./ WT/ ↓	Dimerization interface
Y40C/A, Y47A	B↓ D↓ / B↓ D↓ / ↓	Concave face, fold
L74A	B↓	Buried, fold
Y93A	B↓ / D↓	Buried, fold, hydroxyl group points into concave face, hydrogen bond donor/acceptor
F72L/S/A, F73L/S, C79Y, F108S, I134T	B↓ / D↓	Buried, fold

(B): YopB; (D): YopD; (↓) binding abolished/reduced; (↑): re-established; (-): neither YopB nor YopD; (WT): wild-type; (n.d.) not determined; asterisks designate residues at TPR consensus positions 4/7/11/24/32; conserved sequence residues are underlined.

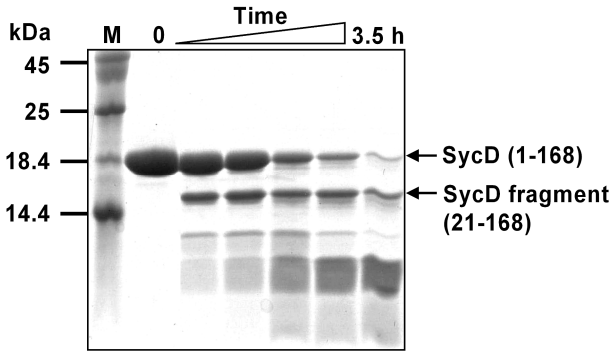

Figure 1

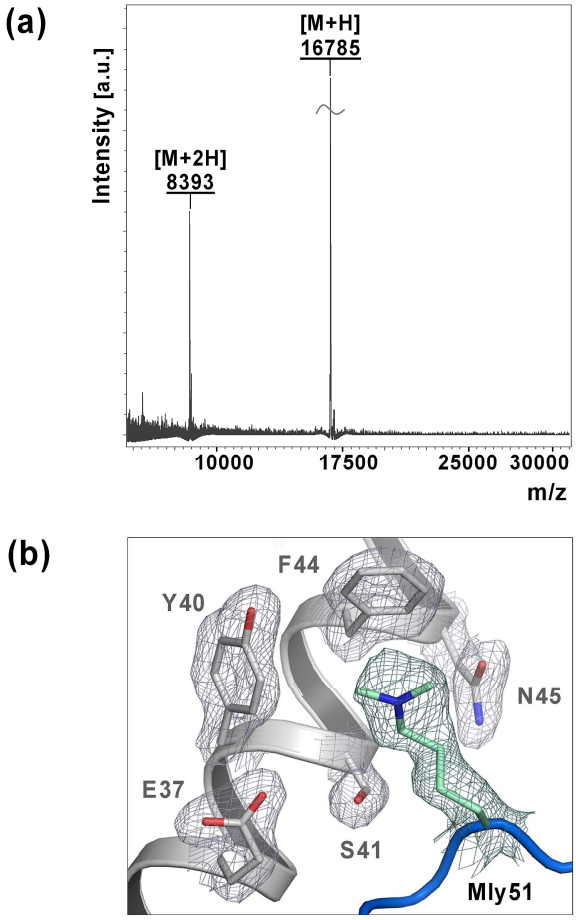
(a)
[M+H]
16785
[M+2H]
8393
Intensity [a.u.]
10000
17500
25000
30000
m/z
(b)
F44
Y40
N45
E37
S41
Mly51

Figure 2

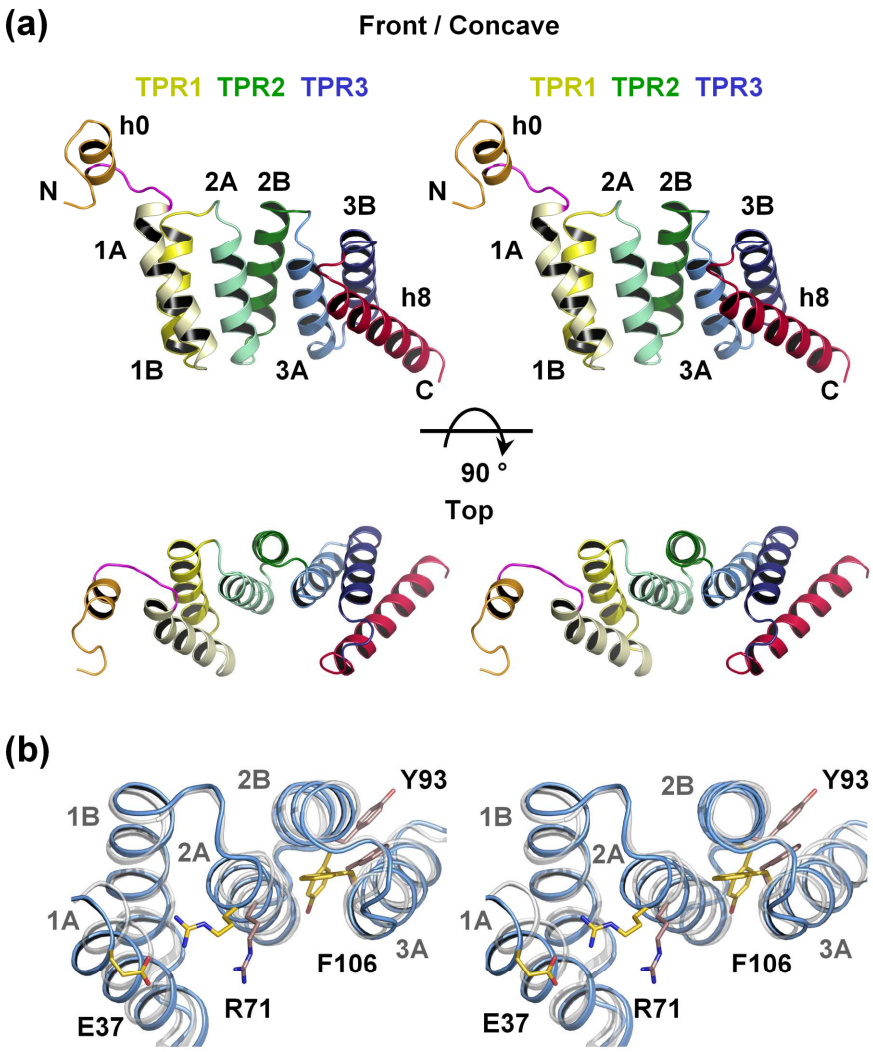
(a)
Front / Concave
TPR1 TPR2 TPR3
TPR1 TPR2 TPR3
h0
N
2A 2B
3B
1A
h8
1B
3A
C
90 °
Top
(b)
2B
Y93
1B
2A
1A
F106
3A
R71
E37

Figure 3

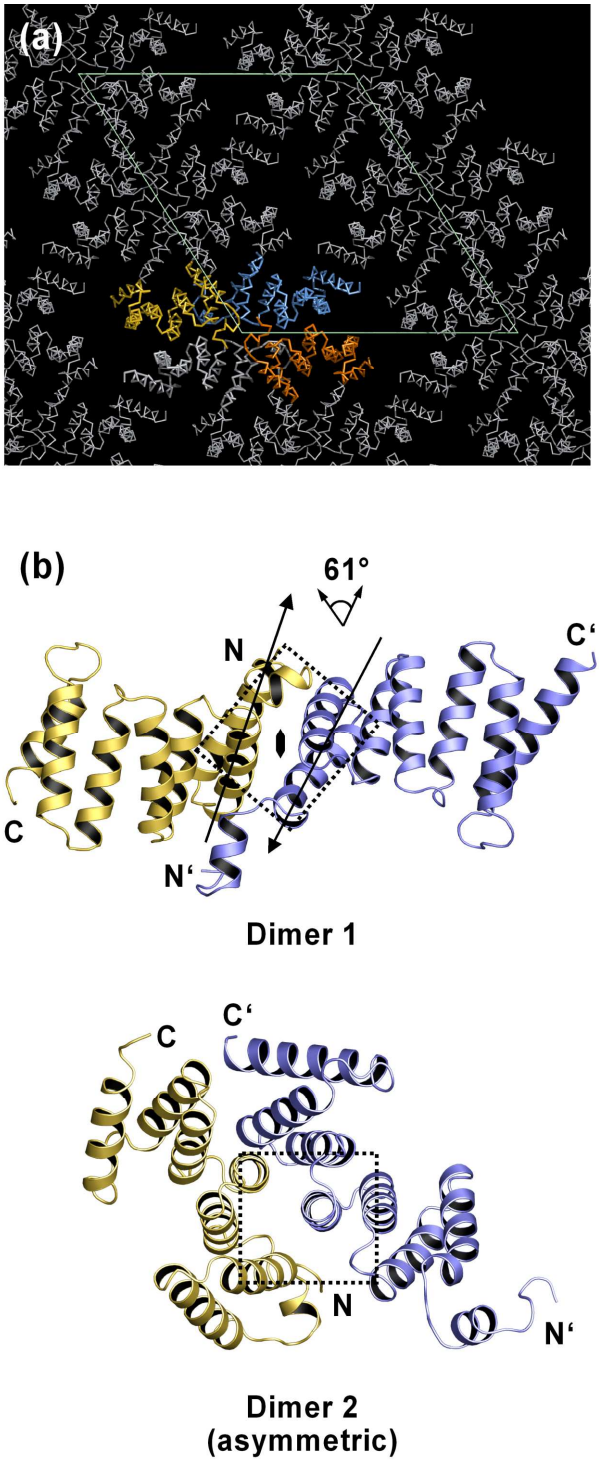

Figure 4

(a)

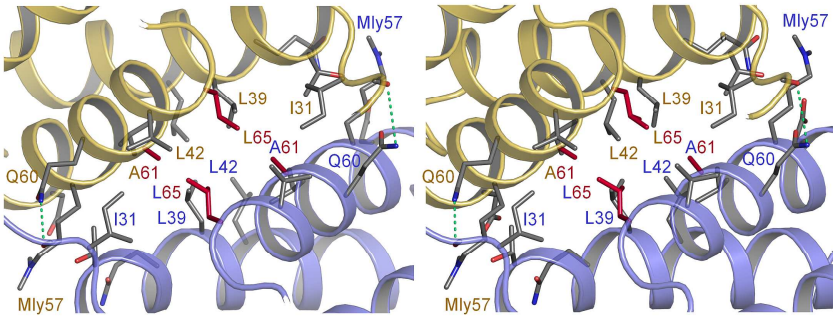
Mly57
L39
I31
L65
A61
L42
Q60
A61
L42
Q60
L65
I31
L39
Mly57
Mly57
L39
I31
L65
A61
L42
Q60
A61
L42
Q60
L65
I31
L39
Mly57

(b)

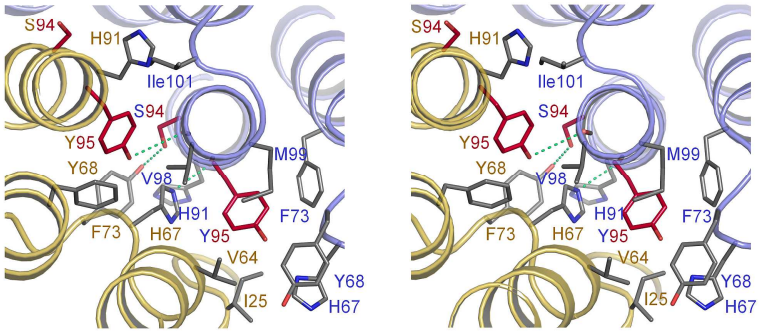
S94
H91
Ile101
S94
Y95
M99
Y68
V98
H91
F73
F73
H67
Y95
V64
Y68
I25
H67
S94
H91
Ile101
S94
Y95
M99
Y68
V98
H91
F73
F73
H67
Y95
V64
Y68
I25
H67

Figure 5

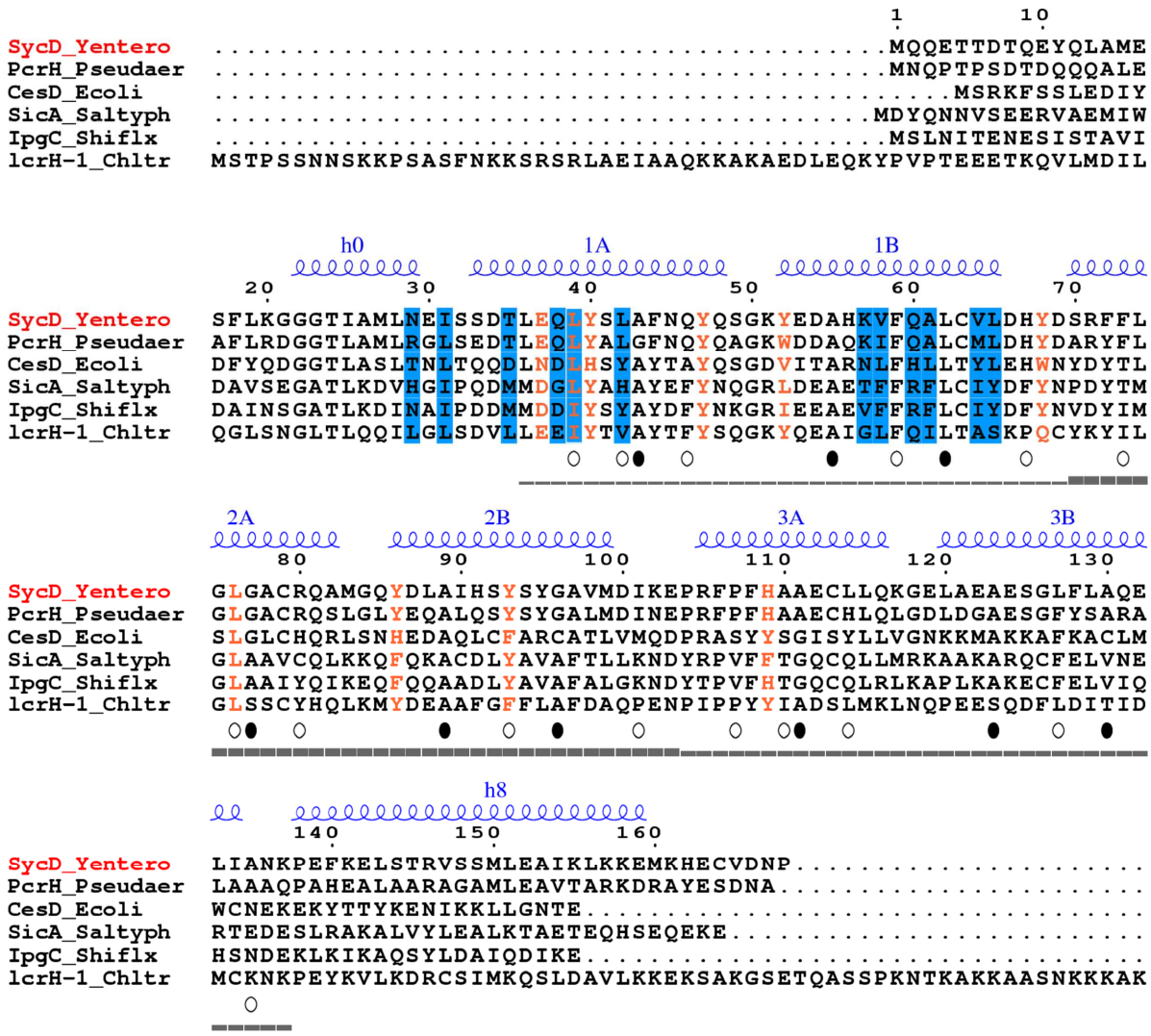
SycD_Yentero
PcrH_Pseudaer
CesD_Ecoli
SicA_Saltyph
IpgC_Shiflx
lcrH-1_Chltr
h0
1A
1B
2A
2B
3A
3B
h8

Figure 6

(a)

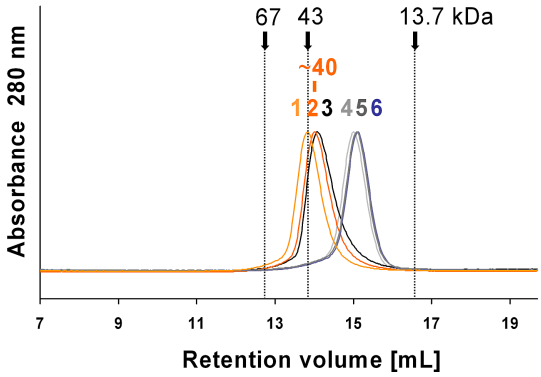

(b)

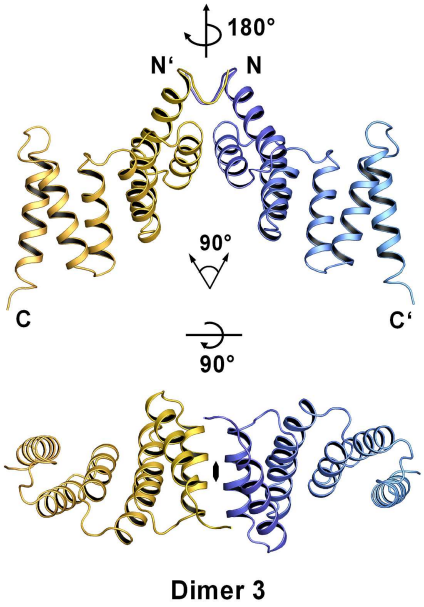

Dimer 3

Figure 7

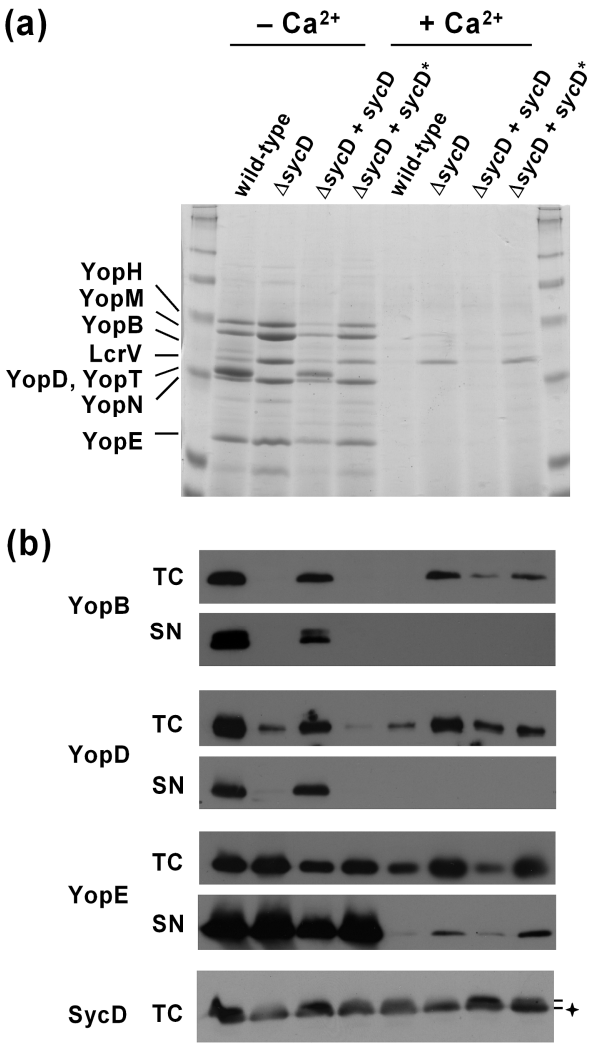
(a)
– Ca2+
+ Ca2+
wild-type
ΔsycD
ΔsycD + sycD
ΔsycD + sycD*
wild-type
ΔsycD
ΔsycD + sycD
ΔsycD + sycD*
YopH
YopM
YopB
LcrV
YopD, YopT
YopN
YopE
(b)
YopB
TC
SN
YopD
TC
SN
YopE
TC
SN
SycD
TC

Figure 8

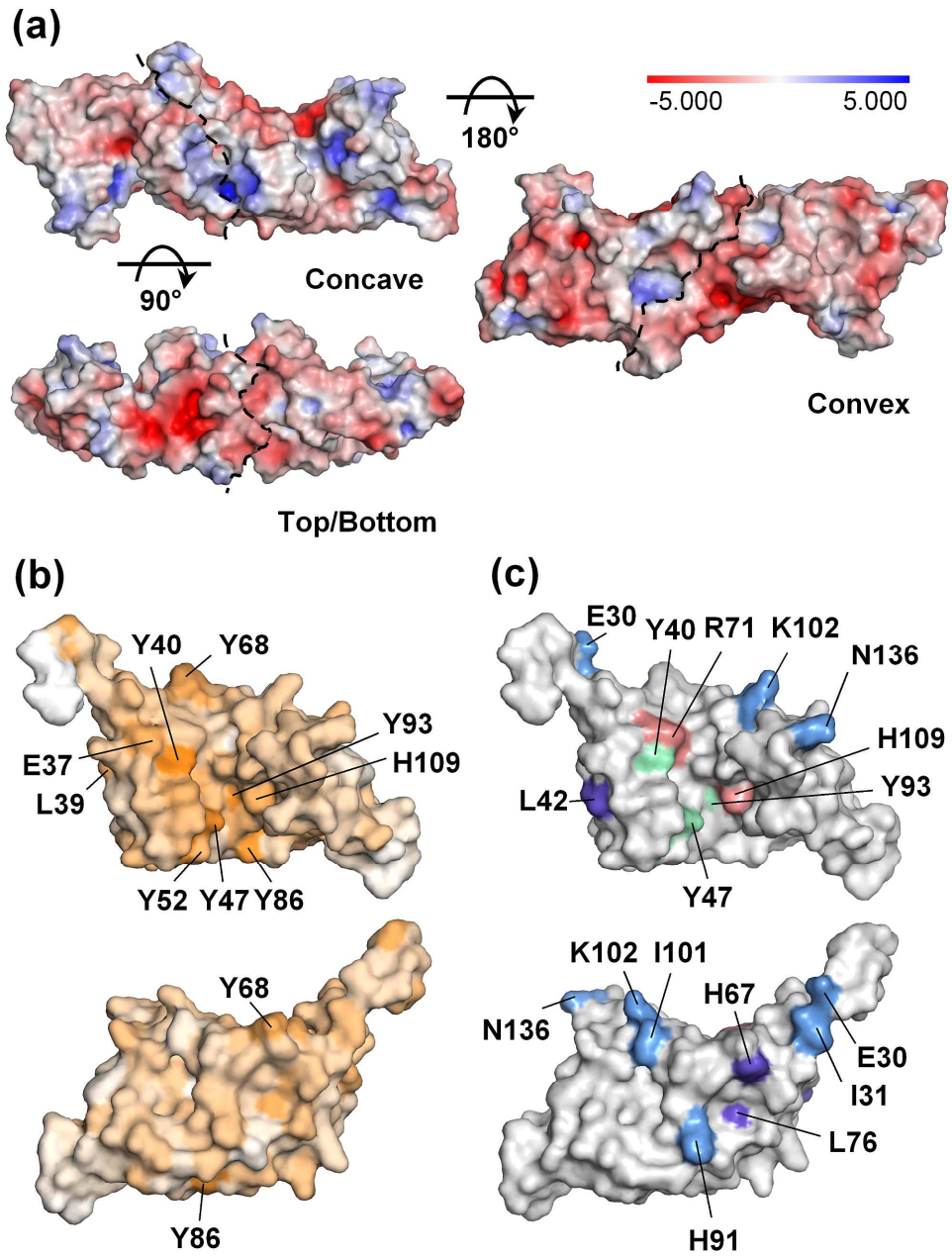
(a)
180°
-5.000
5.000
90°
Concave
Convex
Top/Bottom
(b)
Y40
Y68
Y93
E37
H109
L39
Y52
Y47
Y86
Y68
Y86
(c)
E30
Y40
R71
K102
N136
H109
Y93
L42
Y47
K102
I101
H67
N136
E30
I31
L76
H91

Figure 9